International Journal of Impact Engineering 199 (2025) 105246

Contents lists available at ScienceDirect

International Journal of Impact Engineering

journal homepage: www.elsevier.com/locate/ijimpeng

A novel size distribution model for debris generated by in-orbit collisions

L. Olivieri *, A. Francesconi

Department of Industrial Engineering, University of Padova, Via Venezia 1, 35131, Padova, Italy

ARTICLE INFO

Keywords:
Hypervelocity impact testing
Fragments distribution
Space debris

ABSTRACT

In-orbit fragmentation events can generate debris clouds of thousands of objects, that may strongly affect the debris environment and the management of orbital assets. Ground observations are employed to catalogue detectable objects; however, the observation and identification of the generated debris may require months or even years. Simplified models, such as the NASA Standard Breakup Model, can assess the effects of in-space breakup and promptly provide fragments properties distributions; nevertheless, literature data suggests that they might present some limitations when modern satellite designs or complex impact geometries are involved. In this context, a novel Italian Breakup Model is under development, to provide a more reliable description of the fragmentation events; in particular, a piecewise analytic size distribution equation has been conceived and tuned with both observation data and ground experiments. The model description and its calibration and validation process are reported in this paper; the obtained results show that it accurately captures the trends in experimental and observational data with greater accuracy compared to other existing formulations.

1. Introduction

Space debris represent a growing threat for near-Earth orbits [1,2], as collision velocities make even sub-centimetre objects dangerous for spacecraft subsystems survivability [3] and larger debris may lead to the functional loss and fragmentation of entire vehicles [4]. In addition, the growing trend of orbital launches [5] and the deployment of large constellations [6] are increasing the traffic [7] and the number of resident objects [8], further affecting the Low-Earth Orbits (LEO) and leading to the worrisome configurations forecast by Kessler [9]. In fact, in the last years the number of in-orbit fragmentations has been not negligible [10] in spite of the mitigation strategies implemented by all the involved stakeholders [11–13]. Information on these events is mostly acquired from ground observations [14,15]. Current systems present a minimum resolution limit of about 5 cm for LEO, with larger values for higher orbits; in addition, cataloguing new objects may require different observation with a process that can last weeks or months. In spite of these limits, observations remain the most reliable sources of information on in-space fragmentation [16,17], that can be only in part integrated with data from ground experiments (e.g.: [18–22]).

In this context, it is of paramount importance to understand and model in-space fragmentation events. The understanding of the physical behaviours behind fragments generation and the development of models replicating orbital breakups will help scientists to better simulate the evolution of the debris environment [23,24], engineers to improve debris risk assessment processes [25], and spacecraft operators to assess the dangers arising from debris clouds and untracked fragments to active satellites [26,27]. Numerical [28,29] and semi-empirical [30–32] models allow replicating fragmentation events considering the influence of impact scenarios but often require consistent computational resources and a good knowledge of the involved bodies; on the contrary, empirical models can provide the description of fragments distributions employing simple analytic formulations. Among the latter, the NASA Standard Breakup Model [33] represent the most employed and most known one: it consists of a set of equations describing fragment characteristic length, area-to-mass, and velocity distributions, that were derived from past empirical data collected until the 1990′s. Specifically, the cumulative distribution of characteristic length is presented as a linear trend (in logarithmic space) and depends only on one parameter: the impactor momentum for low-energy sub-catastrophic events, or the overall mass of the involved bodies for high-energy, catastrophic ones [33]. With a threshold set at 40 J/g, the EMR (Energy to Mass Ratio, i.e. the impactor kinetic energy divided by system mass) parameter defines the transition between sub-catastrophic and catastrophic collisions [33]; it shall be mentioned that in the state of the art the threshold has been better defined as a range between 35 J/g and 45 J/g and should be employed in the hypervelocity regime [30]. Thanks to the simplicity of its

* Corresponding author.
E-mail addresses: lorenzo.olivieri@unipd.it (L. Olivieri), alessandro.francesconi@unipd.it (A. Francesconi).

https://doi.org/10.1016/j.ijimpeng.2025.105246
Received 8 November 2024; Received in revised form 23 December 2024; Accepted 31 January 2025
Available online 3 February 2025

formulation, the NASA SBM is employed in the majority of fragmentation tools and debris environment evolution models; however, recent studies suggest that this model may have a few limitations, in particular when modern satellite designs are involved [34]. In addition, it is also known that the SBM is not capable to discern between central and glancing impacts [28,35,36]. Specifically, it has been observed that the inclusion of a corrective coefficient may be necessary to account for the fraction of the satellite involved in the event [37] or to scale the mass of the involved objects to obtain a number of fragments consistent with fragments observations [38].

To address these points, in the last decade the Space Debris Group of the University of Padova has investigated the parameters affecting collisional fragmentations to develop a novel analytic breakup model [39]. The efforts have recently focused on size distributions, thanks to the higher number of experimental and observation data available for this parameter: first, a characteristic lengths cumulative distribution model was proposed, based on numerical simulations [40], and an updated and simplified version was then compared with the real data [41]. In this work, the final characteristic length model is presented, with a summary of the tuning process and the validation against an additional breakup case. The remainder of this paper is organized as follows. Section 2 describes the proposed model and reports the effect of its parameters, while Section 3 presents the experimental and observation data employed for the model tuning and cross-validation. Section 4 describes the tuning process and discusses the main results. Last, Section 5 presents the comparison with additional cases with a partial information on the events.

2. Model description

As mentioned in the introduction, the current size cumulative model from the NASA SBM [33] presents a linear trend (in the logarithmic space); the formulation associates the debris characteristic length L_c (i.e. the average of the object's three orthogonal dimensions) to the cumulative number of fragments N with the following relation:

$$N = 0.1\ M^{0.75} L_c^{-1.71} \tag{1}$$

where M represents the impact momentum for collisions with EMR lower than a threshold of 40 J/g ("sub-catastrophic") and the sum of the involved bodies masses for scenarios with EMR higher of than this value ("catastrophic"). The transition from sub-catastrophic and catastrophic events is therefore non-continuous and it is defined by a fixed threshold, that does not consider the influence of the impact scenario or the characteristics of the involved masses.

The model proposed in this paper tries to overcome this limitation by including a dependence on the collision geometry and involved objects sizes. It is defined by a three-sections piecewise formulation, that can be seen in Fig. 1, representative of three different phenomena that can be observed in the fragmentation of a large objects [40]. In more details, the first section of the curve, labelled as (1), represents the large parts of the involved bodies that survive partially intact to the breakup. The second part, (2), consists of the components detached due to the failure of structural links, such as reaction wheels, or compact or high-density subsystems. Last, the third section, (3), includes the small debris finely fragmented from the elements directly involved in the collision. This trend seems to partly reflect what has been observed through experiments (the flattening of the central section in [42]) and observations (e.g. the different slope of the first section in [43]) and what has been simulated with dedicated software [40].

The model in Fig. 1 can be described by defining only six variables: the coordinates of point A ($L_{c,A}$ and N_A) and the slope of the first section m_1, the coordinates of point B ($L_{c,B}$ and N_B), and the slope of the third section m_3. These six variables are all functions of the following collision scenario parameters [40,41], considering a "target" and an "impactor" objects.

The involved objects size ($L_{c,T}$ and $L_{c,imp}$), the target mass (M_T), and the ratio between the impactor and target cross sections α (which can be calculated as a square of the ratio between their characteristic lengths, see Eq. (2)).

$$\alpha = \left(L_{c,T}/L_{c,imp}\right)^2 \tag{2}$$

These parameters are selected because the fragmentation phenomena seem to be affected by the size of the bodies involved in the fragmentation. In particular, it can be observed that the magnitude of the fragmentation increases with the size of the impactor: the collision of two spacecraft with the same size would generate a different fragmentation with respect to a small projectile impacting on a large satellite.

- The parameter k_1 representing the transition between glancing impact ($k_1 < 1$) and central impact ($k_1 = 1$). The first model presented in [40] addressed discerned central and glancing impacts thanks to a complex formulation to discern between central impacts and "glancing", based on a definition of an "impact angle"; however, observations of events that occurred in orbit cannot give back this type of information, which for a more usable model should be represented by a simpler and more universal scale parameter.
- The collision EMR and the coefficients c_1 and c_2, employed to draw a continuous transitions between sub-catastrophic and catastrophic impacts. As mentioned, the current arbitrary threshold of 40 J/g acts as a rigid split between sub-catastrophic and catastrophic events. In

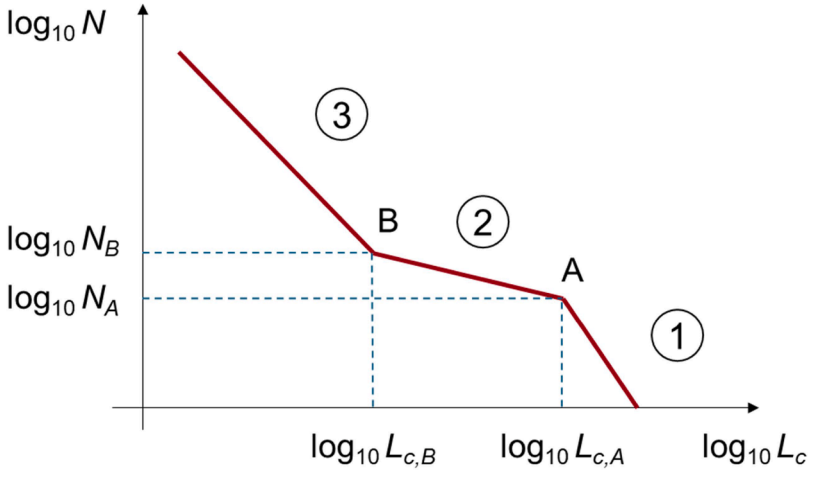

Fig. 1. Three-sections piecewise model for characteristic length cumulative distributions.

fact, it has been observed that the EMR is a good metric for local, non-catastrophic events (values well below 40 J/g) as well as highly catastrophic ones (values well above 100 J/g) [41], but the current threshold is under discussion [4]. Literature data further modelled the effect of EMR on fragments distributions; from the proposed equations it is clear that if the EMR threshold is greatly exceeded the number of fragments is driven up (as visible in the trend of the B parameter in [30]). In this work, two new thresholds are presented, allowing the definition of three main regimes: non-catastrophic collisions, transition regime, and catastrophic events. Fig. 2 shows the graphical representation of the three regions and the two thresholds, as well as the trend of the coefficients c_1 and c_2; as reported in Eqs. (3)-(4), c_1 is equal to 1 for EMRs below TH_1 and grows linearly in the logarithmic space after this threshold, while c_2 is 1 for EMRs above TH_2 and decreases to 0 for values below it.

$$c_1 = \max\left(1, \log_{10}\frac{EMR}{0.1 \cdot TH_1}\right) \tag{3}$$

$$c_2 = \min\left(1,\ \max\left(0, \log_{10}\frac{EMR}{0.1 \cdot TH_2}\right)\right) \tag{4}$$

In the proposed model, no dependence on the impact velocity (i.e. if the collision is in the hypervelocity range) is assumed, as due to the limited amount of tuning data it has been preferred to limit the number of parameters. However, further data may help evaluating the effect of the transition from ballistic to hypervelocity ranges on the fragments distributions.

In the following subsections, the formulation of the equations defining the six variables and the employment of these parameters is provided and the sensitivity of the model to them is presented.

2.1. Model equations

The definition of the three sections of the piecewise curve represented in Fig. 1 can be performed with the following equations. The first branch is defined by three variables: the coordinates of point A ($L_{c,A}$ and N_A) and the slope of the first section m_1. Their formulation is reported in Eqs. (5)–(7):

$$L_{c,A} = c_{LCA} \cdot L_{C,T} \cdot c_1 \tag{5}$$

$$N_A = \max\left(1, \left(\frac{c_{NA}}{\log_{10}(M_T \cdot 1000)} \cdot k_1 \cdot c_1 \cdot (1-\alpha)\right)^{c_2}\right) \tag{6}$$

$$m_1 = -1.71 \cdot c_1 \tag{7}$$

This first branch shows a correction of the slope m_1 with respect to the NASA SBM. In fact, it has been observed that for very energetic events (EMR > 100 J/g, coefficient $c_1 > 1$) a better fragmentation of the satellite occurs, reducing the number of objects with characteristic lengths close to those of the satellite. In addition, with this increase of energy (coefficient $c_1 > 1$) and the consequent improvement of the fragmentation process, the coordinates of point A also tend to lower and move towards larger Lc values, indicating that this branch of the curve tends to shrink and fewer intact parts manage to survive.

Other parameters also influence the value of the ordinate N_A. First, in case of non-central impacts ($k_1 < 1$) or with reduced energies ($c_2 < 1$), the number of fragments generated in this branch of the curve decreases. Second, the transition from collisions with a small impactor to impacts between bodies of comparable size (e.g. the COSMOS-IRIDIUM event [16]) is evaluated through the use of the coefficient α (ratio between areas): for $\alpha = 1$ (objects of similar size) the bodies involved can be fully fragmented and the first branch of the curve degenerates with $N_A = 1$.

With respect to the second branch of the curve, this part is defined by the coordinates of point A and point B ($L_{c,B}$ and N_B), as reported in Eqs. (8)-(9). While point A represents the transition between large parts of the satellite that survived the collision and the components detached for structural failure, point B marks the transition from the latter to the cloud of finely fragmented debris. It shall be noted that microsatellites present proportionally larger components and subsystems with respect to large satellites; for this reason, in the formulation of $L_{C,B}$ two different values of c_{LCB} are proposed as a function of the mass of the satellite. In fact, it can be expected that this branch will be strongly affected by the spacecraft internal structure and compactness; the implementation of these two parameters can help predicting the fragmentation behaviour without including more information on the structure and the internal components.

$$L_{c,B} = \begin{cases} c_{LCB-LARGE} \cdot L_{c,T} & M_T > 1\ kg \\ c_{LCB-SMALL} \cdot L_{c,T} & M_T \leq 1\ kg \end{cases} \tag{8}$$

$$N_B = N_A + \left(EMR^{c-EMR} \cdot k_1 \cdot c_1\right)^{c_2} \tag{9}$$

For the ordinate N_B, the main parameter influencing this equation is the collision EMR. Again, the parameters k_1, c_1 and c_2 affect the formulation in case of "glancing" impacts or high or low energies: central impacts with high energies generate a larger number of fragments with respect to glancing or low-EMR ones.

Last, the third section is defined by point B and by the slope m_3 of this branch. In a similar fashion to the first section, the slope was modelled starting from the initial value proposed by the NASA SBM and applying a correction in function of the target mass and the event EMR. The corrective factors can be seen in Eqs. (10)-(11).

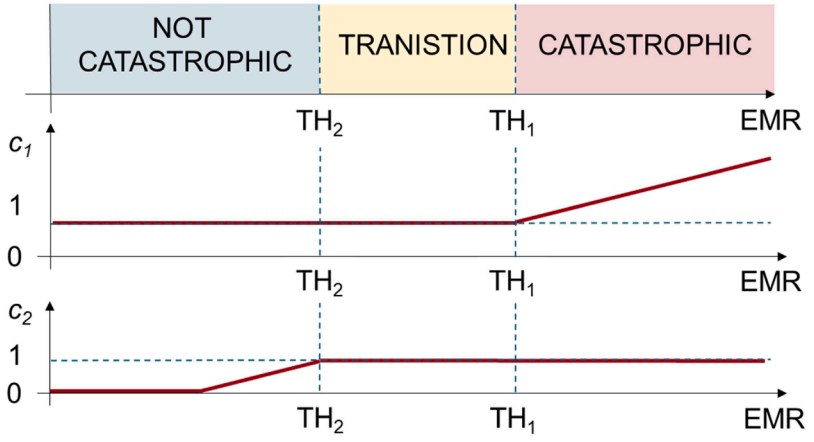

Fig. 2. c_1 and c_2 coefficients trend.

$$\mu_1 = \max\left(1, \log_{10}\left(\frac{M_T}{10}\right)\right) \tag{10}$$

$$\mu_2 = \log_{10}(10 \cdot EMR)/\mu_1 \tag{11}$$

The slope of the third section can be defined as reported in Eq. (12). With this formulation the slope is reduced for low-energy impacts, for which the fine fragmentation of the target areas involved in the collision might be limited.

$$m_3 = \begin{cases} 0 & \mu_2 < 0 \\ -1.71 \cdot \mu_2 & 0 \leq \mu_2 < 1 \\ -1.71 & \mu_2 \geq 1 \end{cases} \tag{12}$$

For sake of completeness, the values of the tuning coefficients can be seen in Table 1; however, the tuning process that led to these results is detailed in Section 4.

2.2. Model sensitivity to input parameters

In this subsection the sensitivity of the model over the main input parameters is assessed by evaluating one by one the influence of EMR, target mass, cross sections ratio, and impact geometry (coefficient k_1). A graphical representation of this analysis can be seen in Fig. 3; in all plots for the reference curve (green solid line) the parameters are EMR= 1E6 J/kg, M_T=100 kg, α=0.5, and k_1=1. In addition, all plots present the normalized characteristic length ($L_c/L_{c,T}$) on the x-axis, and the cumulative number of fragments on the y-axis.

From the top left plot, it is evident that increasing the EMR leads to an increase in the number of fragments. Additionally, above the threshold TH_1 (that influences the coefficient c_1) the x-value of point A translates to higher characteristic lengths with a lower further increase in the number of generated fragments; this results in a steeper trend for the first branch of the distribution. In fact, this model assumes that an energetic event is more effective in finely fragment the spacecraft: the increase in the number of large pieces will slow down after the TH_1 threshold, even while the total number of fragments is constantly growing. Last, it can be observed that for low values of the EMR, representing low-energy collisions, even the slope of third branch of the curve (small fragments) decreases.

The effect of the target mass (bottom left) appears to be less significant for large objects (i.e. with mass $>$ 1 kg), as all the curves almost overlap. This suggests that there is little correlation between the target mass and the mechanisms causing the fragmentation. It should be noted, nonetheless, that this trend is normalized on the x-axis ($L_c/L_{c,T}$) in the figure. Taking into account a relationship between the target mass and size, it is evident that the curves translate to larger values of L_c as M_T increases. Smaller objects (with mass $\leq$ 1 kg) show a different behaviour for the second and third branches: following Eq. (8), the x-axis coordinate of point B is translated to a larger value, as small satellites present a different internal layout with proportionally larger components that the fragmentation event may detach.

The cross section α (top right) has a strong influence on the first branch of the curve. It has been found that collisions between objects of similar dimensions (α close to 1) are more effective at fragmenting the entire target, producing only small debris, whereas small impactors (small values of α) produce a less efficient fragmentation, with large parts of the spacecraft detaching. The first branch of the suggested model collapses to the x-axis for α= 1.

Last, decreasing the coefficient k_1 (bottom right) scales down the curve: a central impact (k_1= 1) generates the largest number of fragments (reference case, solid red line) while for glancing ones the generated objects drastically decrease.

In summary, it can be observed that the proposed model represents the effect of the different collision parameters, depicting a reasonable variation of the characteristic length cumulative distributions.

Table 1
Tuning coefficients.

Coefficient	Value
TH_1 [J/g]	140.75 ± 43.80
TH_2 [J/g]	43.79 ± 1.41
c_{LCA}	0.1276 ± 0.0030
c_{NA}	255.96 ± 1.91
$c_{LCB-LARGE}$	0.0085 ± 0.0018
$c_{LCB-SMALL}$	0.0405 ± 0.0015
c_{EMR}	0.6230 ± 0.0201

3. Tuning data

To obtain the tuning coefficients reported in Table 1, a set of both experimental and observation data was employed. Table 2 lists the 12 dataset employed in this work, with the literature reference, the classification (experiment or observation), the EMR, and the distinction between central and glancing impact. In particular, due to the limited available information, only three observations are included in the table: the COSMOS 2251 – IRIDIUM 33 collision [16], with a dataset for each spacecraft, and the COSMOS 1408 anti-satellite test [43]. Experimental data are related to the work of different research groups: two tests from Hanada [35], employing cubic targets with edge size of 20 cm and internal composite plates to simulate boards and subsystems, three tests from Lan [42], using 40 cm^3 cubic mock-ups with internal aluminium boxes and plates, two tests on picosatellites with various materials and internal components [22,44], one on a 2 U CubeSat model [21], and the 56 kg DEBRISAT representative satellite model [20]. Among all cases, EMRs values vary from 19 J/g to >100,000 J/g.

4. Model tuning

The model tuning and pre-validation process was developed considering the small available dataset. For this reason, a dedicated procedure was employed to use smaller subsets of data and cross-validate them with the remaining experiments and observations; this also allowed the determination of an uncertainty range to apply to the model tuning coefficients. In this section, a detailed description of the procedure and of the collected results is reported.

First, a metric was defined to evaluate the quality of the model with respect to experimental and observational distributions. The model error was calculated as the sum of the norm of the deviations from the expected distribution, defined in terms of $\log_{10}N$, and sampled on 50 equidistant values of $\log_{10}L_C$. In the case of more than one distribution, the error was normalized on the number of dataset. A maximal threshold of 2 was also defined; errors larger than this value indicate that the model does not accurately represent the real-case data.

Second, the whole dataset was divided into 7 cases, visible in Table 3; for each case, two groups of data were created, one as “tuning dataset”, the other as "cross-validation dataset”. With the exception of the first case, that included all data in both groups, for each case at least one family of experiments or observations was moved from the tuning to the cross-validation group.

Third, for each of the model tuning coefficients, starting from an initial value, defined in the original model reported in [41], a tuning range was defined (see Table 4, columns 2 and 3). Inside each range, the probability of the possible values was defined by a continuous uniform distribution.

Fourth, for each case, a Montecarlo of 10,000 simulations was performed, with the tuning coefficient randomly sourced from the tuning range; the combination of coefficients minimizing the error was taken as the best one for that case. In Table 4, columns 4 to 10, the values of the seven combinations can be found, as well as the tuning error.

Fifth, for each case, the chosen set of coefficients was employed for the cross-validation with the selected dataset; again, the model error was calculated (see Table 4, last row) and for each case it is also reported in

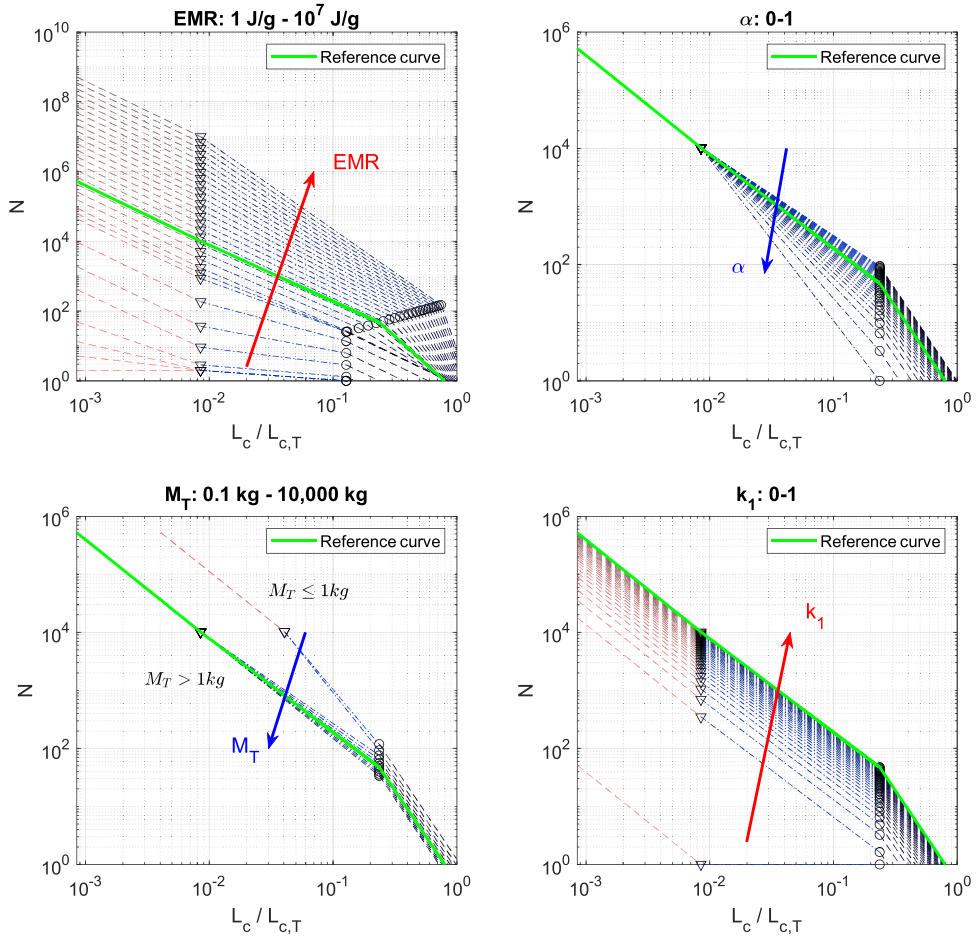

Fig. 3. Sensitivity analysis on the input parameters.

Table 2
Data employed for model calibration.

N.	Target	REF	Experiment / observation	EMR, J/g	Central/ glancing
01	HANADA–HVI	[35]	Experiment	52	Central
02	HANADA–LVI	[35]	Experiment	61	Central
03	LAN–01	[42]	Experiment	71	Central
04	LAN–02	[42]	Experiment	55	Central
05	LAN–03	[42]	Experiment	48	Central
06	PICOSAT–01	[22]	Experiment	78	Central
07	PICOSAT–02	[44]	Experiment	78	Glancing
08	COSMOS 1408	[43]	Observation	907	Central
09	CNES	[21]	Experiment	19	Central
10	DEBRISAT	[20]	Experiment	235	Central
11	COSMOS 2251	[16]	Observation	41,564	Central
12	IRIDIUM 33	[16]	Observation	108,906	Glancing

Table 3
Tuning and cross-validation cases.

Case number	Case name	Tuning datasets	Cross-validation datasets
1	All	1–12	1–12
2	No HANADA	3–12	1–2
3	No LAN	1–2, 6–12	3–5
4	No PICOSAT	1–5, 8–12	6–7
5	No COSMOS 1408	1–7, 9–12	8
6	No CNES and DEBRISAT	1–8, 11–12	9–10
7	No COSMOS-IRIDIUM	1–10	11–12

Fig. 4. The cases with an cross-validation error larger than 2 were then discharged, leaving only cases 1 to 4 for further evaluation.

Last, the coefficients values and uncertainties were obtained by calculating the mean and the standard deviation of the values from the selected cases. The final values are reported in the last column of Table 4.

Among the resulting values, it can be observed that the majority of the tuning coefficients present an uncertainty below 5 % of the average value; this suggests that the model can reliably represent the different collision scenarios employed in the tuning process and that the main relations among the parameters are well identified. The two exceptions to this behaviour are represented by TH_1 and by $c_{LCB-LARGE}$, that present larger deviations; in the first case it shall be noted that among the available dataset the EMRs were all well below or above this value, limiting the capacity of the tuning process to identify a well defined threshold. It is expected that with additional data around this value a reduction of the coefficient uncertainty could be obtained. With respect to $c_{LCB-LARGE}$, it shall be considered that a large number of the experiments employed equivalent plates or boxes instead of the real spacecraft subsystems; this could affect the size of the detached parts and therefore the value of this coefficient. Again, it is expected that new experiments on more representative models might lead to the reduction of this uncertainty.

Fig. 5 shows the application of the model with the final value of the tuning coefficients to the 12 dataset. The two glancing impacts, PICOSAT-02 (collision on the center of one edge of the cubic shape) and IRIDIUM 33 (a non-central collision involving the spacecraft appendage), were modelled by imposing a coefficient value for k_1 of 1/3 and 1/4, respectively.In all cases it can be observed that the proposed

Table 4
Tuning coefficients.

Coefficient	Initial value [41]	Tuning range	Case 1	Case 2	Case 3	Case 4	Case 5	Case 6	Case 7	Final value
TH_1 [J/g]	100	50–150	148.86	116.39	148.86	148.86	135.16	140.07	148.86	140.75 ± 16.24
TH_2 [J/g]	40	20–60	44.49	41.68	44.49	44.49	41.76	29.70	44.49	43.79 ± 1.41
c_{LCA}	0.1	0.08–0.13	0.1291	0.1231	0.1291	0.1291	0.1237	0.1264	0.1291	0.1276 ± 0.0030
c_{NA}	355	200–400	256.92	253.10	256.92	256.92	300.63	294.15	256.92	255.96 ± 1.91
$c_{LCB-LARGE}$	0.01	0.003–0.03	0.0093	0.0058	0.0093	0.0093	0.0093	0.0066	0.0093	0.0085 ± 0.0018
$c_{LCB-SMALL}$	0.05	0.02–0.09	0.0413	0.0382	0.0413	0.0413	0.0471	0.0400	0.0413	0.0405 ± 0.0015
c_{EMR}	0.58	0.4–0.7	0.6129	0.6532	0.6129	0.6129	0.5949	0.6310	0.6129	0.6230 ± 0.0201
Tuning error			1.6907	1.7180	1.8960	1.8001	1.6121	1.5713	1.4944	
Cross-validation error			1.6907	1.6997	1.0749	0.5475	2.8125	3.2437	2.6721	

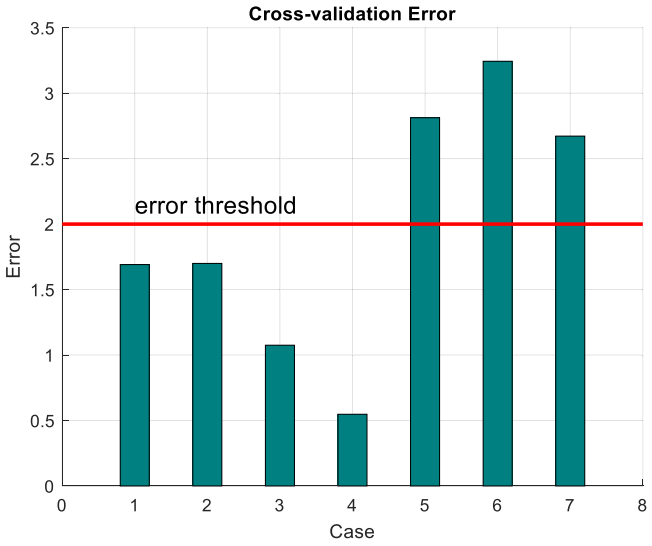

Fig. 4. Cross-validation errors for coefficients tuning.

model (brown dash-dot line) is more capable in fitting the real data (black solid line) with respect to the NASA SBM (blue dashed line).

With respect to the experiments, the DEBRISAT distribution and the Lan test data clearly exhibit the three-sections trend. The model's accuracy appears to be lower when it comes to the data from Hanada, but the NASA SBM exhibits a similar pattern for these experiments. Last, the differing transition threshold between Sections 2 and 3 is consistent with the experimental distributions for smaller targets (Picosatellite tests and CNES experiment), indicating that the assumption about the characteristic size of the components of a small satellite may be accepted.

Regarding observations, the model shows that it can reconstruct the higher slope of the first portion of the fragments distributions for the COSMOS 1408 anti-satellite test; it also generally follows the observation distribution trend. The model is more representative of the NASA SBM in both scenarios for the COSMOS-IRIDIUM event when the scale factor for glancing is assumed for the IRIDIUM 33 case. It can be noted that the event EMR for these two distributions is several orders of magnitude greater than in the earlier dataset. This causes the model's initial section to collapse, as it is expected that no large parts of the two satellites survived the event intact.

5. Model comparison with additional events

A further evaluation of the model performance was performed with two additional dataset (see Table 5) for which the information on the events were only partial.

The first dataset refers to the anti-satellite test of January 11, 2007, on the FENGYUN 1C defunct meteorological spacecraft [45]. The satellite had a $1.5 \times 1.5 \times 1.5$ m^3 cubic shape with two 4-meters long solar panels and a mass of 954 kg [46]; the impact velocity was reconstructed at 9.36 km/s [45]. However, literature data is not consistent on the kinetic impactor size and mass; considering other ASAT tests, in this paper a value of 100 kg for the vehicle mass is inferred and, additionally, a sensibility analysis is performed on this parameter. The event led to the generation of thousands of fragments directly observable from ground telescopes, with an estimation of >100,000 uncatalogued debris larger than 1 cm [47]. Literature data on fragments characteristic length distributions is limited to 2500 objects larger than 5 cm [48].

Fig. 6 compares the observation data with the NASA SBM (blue) and the proposed model (brown) both for the reference value of 100 kg for the impactor mass (thick lines) and for a range from 1 kg to 1000 kg (thin lines). It can be seen that the mass variation does not substantially influence the NASA SBM trend, with only a small increase in the line intercept, that depends only on the total mass (i.e. the sum of the satellite and the impactor mass); for all cases, and in particular for the objects larger than 1 m, the NASA SBM underestimates the majority of the observation distribution trend. The proposed model, for the reference impactor mass, can better follow this initial part, due to a higher slope of its first section with respect to the NASA SBM. In the second section, it overestimates the medium-range debris, in particular around the size of 30 cm; however, the observed fragments number quickly increases below this value, reducing the gap between model and the observations. Below 10 cm the observation resolution is reached and only a few fragments were catalogued, not allowing any evaluation on the third section of the model.

The influence of the impactor mass (and consequently of the collision EMR) on the model trend is clearly recognizable. The number of generated fragments increase with the mass: as reference, in this collision configuration, for the proposed model a 1 kg projectile would create 10 objects larger than 1 m, while a 1000 kg impactor would generate, in the same class, >400 objects. This result underlines how the proposed model has been designed to consider the effect of the different impact parameters.

The second dataset is related to the SOCIT4 "Oscar" fragmentation experiment from 1992 [49], that involved a real satellite bus equipped with the majority of its subsystems. The test data was fundamental for the development of the NASA SBM for the low and intermediate size fragments [33]. The 35 kg satellite was hit by a 4.7 cm spherical aluminium projectile (mass of 150 g) at a velocity of 6.1 km/s, generating a large number of fragments from the different materials. Data on SOCIT cumulative distributions available in literature is mostly limited to the mass [50]; however, it was possible to employ the size-mass distributions presented by Krisko to extrapolate fragments characteristic lengths for the objects larger than 1 cm [49].

The comparison of SOCIT data with the NASA SBM and the proposed model can be seen in Fig. 7. It can be observed that the NASA SBM generally overestimate the number of fragments; on the contrary, the proposed model identifies both the intercept with the x-axis and the presence of a change in the trend slope. While it slightly underestimates the central part of the distribution (around 10 cm), the deviation is limited to few tens of fragments. Again, the available data range could not be used to evaluate the trend of the third section of the model.

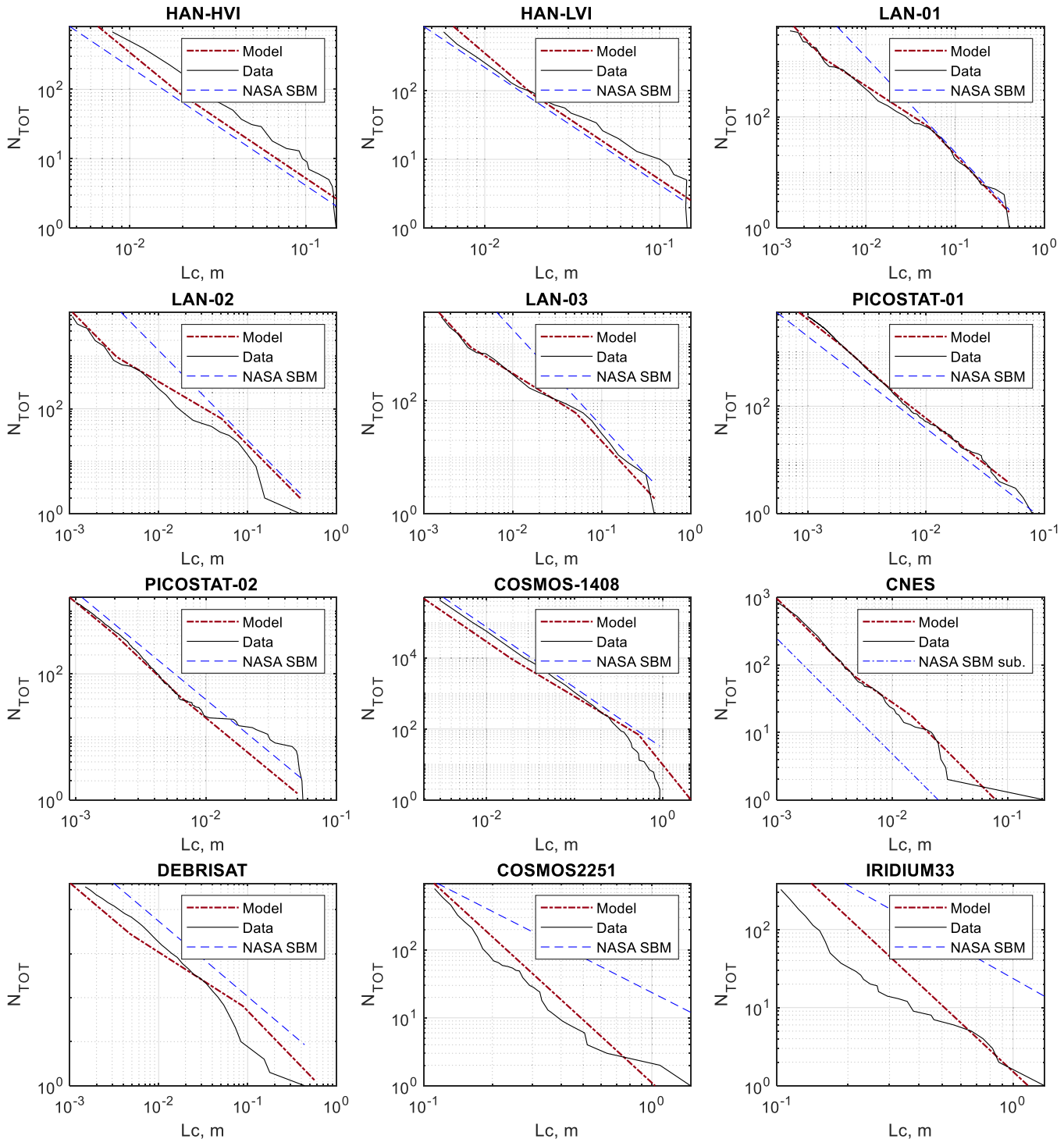

Fig. 5. Comparison of the model (brown dashed-dotted line) with experimental and observation data (black solid line) and with the NASA SBM (blue dashed line).

Table 5
Data employed for model comparison with additional events.

N.	Target	REF	Experiment / observation	EMR, J/g	Central/ glancing
V1	FENGYUN 1C	[45–48]	Observation	Unknown	Central
V2	SOCIT4	[49]	Experiment	80.89	Central

6. Conclusions

This paper presented a three-sections piecewise model for space debris characteristic length cumulative distributions from in-orbit collisions. With respect to the NASA SBM, it employs a larger number of input parameters to better define the influence of the collision geometry on the generation of fragments. The influence of such parameters on the model results is also evaluated through a sensitivity analysis, showing the effect of the EMR, the target mass, the involved objects cross section, and the impact geometry (in terms of the parameter k_1, representing the transition from glancing to central impacts).

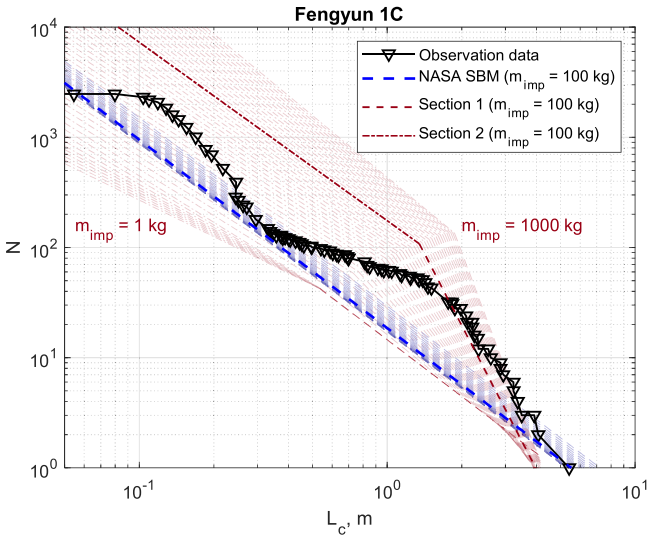

Fig. 6. FENGYUN 1-C observation data (black markers) compared with the model (brown dashed-dotted lines) and with the NASA SBM (blue dashed lines) varying the impactor mass. The reference case (thick lines) consider a 100 kg impactor.

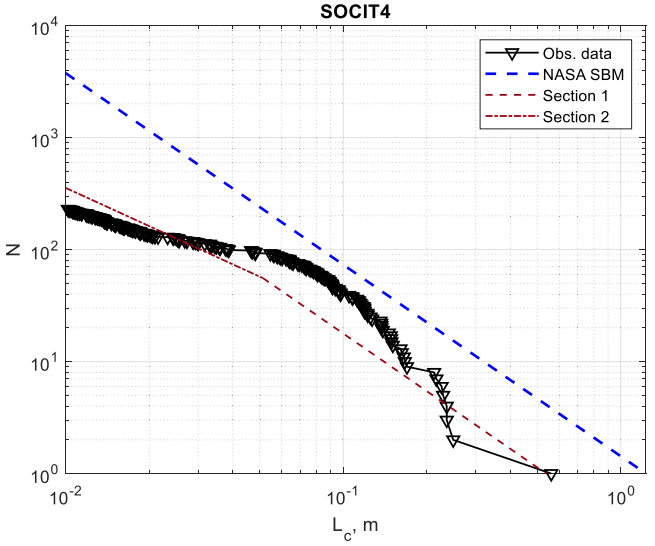

Fig. 7. Comparison of SOCIT data (black markers) with the proposed model (brown dashed-dotted line) and with the NASA SBM (blue dashed line).

The model was calibrated employing both observations of in-space break-up events and ground experiments on spacecraft mock-ups; results confirm the existence of a transition from sub-catastrophic to catastrophic impacts, finding a EMR threshold close to the well-known value of 40 J/g, but suggests the existence of an intermediate regime up to 140 J/g.

The current formulation is capable of reconstructing the employed distribution with only small deviations; it is expected that the employment of new data might be employed for updating the model tuning coefficients and further improving its reliability. The application to two additional dataset confirmed that the proposed model is more capable than the NASA SBM in replicating the fragments characteristic length cumulative distributions.

Future activities foresee the development of companion models both for the area to mass and the velocity distributions, to obtain a fully functional Italian Breakup Model, capable to provide a more reliable description of ins-space fragmentation events. This activity will require the acquisition of more dataset on both parameters, that will be collected both from observations of new in-space collisions and ground experiments.

CRediT authorship contribution statement

L. Olivieri: Writing – original draft, Validation, Software, Investigation, Formal analysis. **A. Francesconi:** Supervision, Methodology, Funding acquisition, Conceptualization.

Declaration of competing interest

The authors declare that they have no known competing financial interests or personal relationships that could have appeared to influence the work reported in this paper.

Acknowledgments

This work has been executed in the framework of ASI project 2023-37-HH.0 “Attività tecnico-scientifiche di supporto a C-SSA/ISOC e simulazione di architetture di sensori per SST”.

Data availability

Data will be made available on request.

References

[1] Johnson NL. Orbital debris: the growing threat to space operations. In: 33rd Annual Guidance and Control Conference; 2010. No. AAS 10-011.
[2] Murtaza A, Pirzada SJH, Xu T, Jianwei L. Orbital debris threat for space sustainability and way forward. IEEE Access 2020;8:61000–19.
[3] Adushkin VV, Aksenov OY, Veniaminov SS, Kozlov SI, Tyurenkova VV. The small orbital debris population and its impact on space activities and ecological safety. Acta Astronaut 2020;176:591–7.
[4] Pardini C, Anselmo L. Review of past on-orbit collisions among cataloged objects and examination of the catastrophic fragmentation concept. Acta Astronaut 2014; 100:30–9.
[5] Letizia Francesca, Virgili Benjamin Bastida, Lemmens Stijn. Assessment of orbital capacity thresholds through long-term simulations of the debris environment. Advances in Space Research 2022.
[6] Olivieri L, Francesconi A. Large constellations assessment and optimization in LEO space debris environment. Adv Space Res 2020;65:351–63.
[7] Rossi A, Sánchez-Ortiz N, David E, Opromolla R, Grishko D. Future activities in the Near-Earth space in the face of ever-increasing space traffic. Acta Astronaut 2024.
[8] Letizia F, Virgili BB, Lemmens S. Assessment of orbital capacity thresholds through long-term simulations of the debris environment. Adv Space Res 2023;72(7): 2552–69.
[9] Kessler DJ, Cour-Palais BG. Collision frequency of artificial satellites: the creation of a debris belt. J Geophys Res Space Phys 1978;83:2637–46.
[10] Anz-Meador P, Opiela J, Liou JC. History of on-orbit satellite fragmentations. 2023. NASA/TP-20220019160.
[11] Stokes H, Akahoshi Y, Bonnal C, Destefanis R, Gu Y, Kato A, Tang M. Evolution of ISO’s space debris mitigation standards. J Space Safety Eng 2020;7(3):325–31.
[12] Migaud MR. Protecting earth’s orbital environment: policy tools for combating space debris. Space Policy 2020;52:101361.
[13] Soares T, Morales Serrano S, Cattani BM, de Courson SA. ESA’s zero debris approach: a responsible path to mitigate space debris in valuable orbits. LPI Contrib 2023;2852:6059.
[14] Mehrholz D, Leushacke L, Flury W, Jehn R, Klinkrad H, Landgraf M. Detecting, tracking and imaging space debris. ESA Bull 2002;(109):128–34. *0376-4265*.
[15] Karamanavis V, Dirks H, Fuhrmann L, Schlichthaber F, Egli N, Patzelt T, Klare J. Characterization of deorbiting satellites and space debris with radar. Adv Space Res 2023;72(8):3269–81.
[16] Kelso TS. Analysis of the Iridium 33-Cosmos 2251 collision. Adv Astronaut Sci 2009;135(2):1099–112.
[17] Pardini Carmen, Anselmo Luciano. Assessment of the consequences of the Fengyun-1C breakup in low Earth orbit. Adv Space Res 2009;44(5):545–57.
[18] Hanada T, Liou JC. Comparison of fragments created by low-and hyper-velocity impacts. Adv Space Res 2008;41(7):1132–7.
[19] Lan SW, Liu S, Li Y, Ke FW, Huang J. Debris area distribution of spacecraft under hypervelocity impact. Acta Astronaut 2014;105(1):75–81.
[20] Murray J, Cowardin H, Liou JC, Sorge M, Fitz-Coy N, Huynh T. Analysis of the DebriSat fragments and comparison to the NASA standard satellite breakup model. In: International Orbital Debris Conference (IOC); 2019. No. JSC-E-DAA-TN73918.
[21] Abdulhamid H, Bouat D, Collé A, Lafite J, Limido J, Midani I, Omaly P. On-ground HVI on a nanosatellite. Impact test, fragments recovery and characterization,

impact simulations. In: Proceedings of the 8th ESA Space Debris Conference20; 2021.
[22] Olivieri L, Smocovich PA, Giacomuzzo C, Francesconi A. Characterization of the fragments generated by a Picosatellite impact experiment. Int J Impact Eng 2022; 168:104313.
[23] Rossi A, Anselmo L, Cordelli A, Farinella P, Pardini C. Modelling the evolution of the space debris population. Planet Space Sci 1998;46(11–12):1583–96.
[24] Dolado-Perez JC, Pardini C, Anselmo L. Review of uncertainty sources affecting the long-term predictions of space debris evolutionary models. Acta Astronaut 2015; 113:51–65.
[25] Canoy J, Bettinger R. Preliminary debris risk assessment for mega-constellations in low and medium earth orbit due to satellite breakup. J Defense Model Simul 2023: 15485129231163868.
[26] Seong JD, Kim HD. Optimization of collision avoidance maneuver planning for cluster satellites in space debris explosion situation. Proc Instit Mech Eng Part G J Aerospace Eng 2018;232(3):407–22.
[27] Oltrogge D, Cooper J. Space Situational awareness and Space traffic management. Space Debris Peril: Pathways Opport 2020;9.
[28] Schimmerohn M, Matura P, Watson E, Durr N, Altes A, Cardone T, Schaefer F. Numerical investigation on the standard catastrophic breakup criteria. Acta Astronaut 2021;178:265–71.
[29] Springer HKeo, et al. Satellite collision modeling with physics-based hydrocodes: debris generation predictions of the iridium-cosmos collision event and other impact events. no. LLNL-CONF-454151. Livermore, CAUnited States: Lawrence Livermore National Lab.(LLNL); 2010.
[30] McKnight D, Maher R, Nagl L. Refined algorithms for structural breakup due to hypervelocity impact. Int J Impact Eng 1995;17(4–6):547–58.
[31] Sorge ME, Mains DL. IMPACT fragmentation model developments. Acta Astronaut 2016;126:40–6.
[32] Francesconi A, Giacomuzzo C, Olivieri L, Sarego G, Duzzi M, Feltrin F, de Wilde D. CST: a new semi-empirical tool for simulating spacecraft collisions in orbit. Acta Astronaut 2019;160:195–205.
[33] Johnson NL, Krisko PH, Liou JC, Anz-Meador PD. NASA's new breakup model of EVOLVE 4.0. Adv Space Res 2001;28(9):1377–84.
[34] Olivieri Lorenzo, et al. Simulation of in-space fragmentation events. Aerotecnica Missili & Spazio 2023:1–8.
[35] Hanada Toshiya, et al. Outcome of recent satellite impact experiments. Adv Space Res 2009;44(5):558–67.
[36] Pardini Carmen, Anselmo Luciano. Review of the uncertainty sources affecting the long-term predictions of space debris evolutionary models. In: Proceedings of the 3rd European workshop on space debris modelling and remediation. Paris: CNES Headquarters; 2014.
[37] Francesconi Alessandro, et al. Numerical simulations of hypervelocity collisions scenarios against a large satellite. Int J Impact Eng 2022;162:104130.
[38] Cimmino N, Isoletta G, Opromolla R, Fasano G, Basile A, Romano A, Cecchini A. Tuning of NASA standard breakup model for fragmentation events modelling. Aerospace 2021;8(7):185.
[39] Olivieri L, Giacomuzzo C, Lopresti S, Francesconi A. Research at the University of Padova in the field of space debris impacts against satellites: an overview of activities in the last 10 years. Appl Sci 2023;13(6):3874.
[40] Olivieri L, Giacomuzzo C, Francesconi A. Simulations of satellites mock-up fragmentation. Acta Astronaut 2023;206:233–42.
[41] Olivieri L, Francesconi A. A new characteristic length debris distribution model for in-space collision events. In: 75th International Astronautical Congress; 2024. 10-.
[42] Lan Sheng-wei, et al. Debris area distribution of spacecraft under hypervelocity impact. Acta Astronaut 2014;105(1):75–81.
[43] Cerutti-Maori D, Carloni C, Rosebrock J, Siminski J. Observation of cosmos-1408 debris cloud with the tracking and imaging radar system. In: Proc. 2nd NEO and Debris Detection Conference; 2023.
[44] Lopresti S, Olivieri L, Giacomuzzo C, Francesconi A. In: Hypervelocity impact testing and simulation at the University of Padova, in proceedings of 17th HVIS; 2024.
[45] Pardini Carmen, Anselmo Luciano. Assessment of the consequences of the Fengyun-1C breakup in low Earth orbit. Adv Space Res 2009;44(5):545–57.
[46] https://space.skyrocket.de/doc_sdat/fy-1.htm (last access: 04-11-2024).
[47] Matney M, Stansbery E, Liou J-C, Stokely C, Horstman M, Whitlock D. Measurements of the small particle debris cloud from the 11 January 2007 Chinese anti-satellite test. In: Proceedings of the 59th International Astronautical Congress; 2008. September.
[48] Stansbery Gene, et al. A comparison of catastrophic on-orbit collisions. In: 2008 AMOS Conference; 2008. September.
[49] Krisko PH, Horstman M, Fudge ML. SOCIT4 collisional-breakup test data analysis: with shape and materials characterization. Adv Space Res 2008;41(7):1138–46.
[50] Maethner SR. Correlation of empirical spacecraft breakup model's predictions with data from hypervelocity impact experiments. Space debris detection and mitigation, 1951. SPIE; 1993. p. 86–97.